MULTISCALE MODELING OF EQUAL CHANNEL ANGULAR EXTRUDED ALUMINIUM WITH STRAIN GRADIENT CRYSTAL PLASTICITY AND PHENOMENOLOGICAL MODELS

L. Duchêne[‡], M.G.D. Geers[§], W.A.M. Brekelmans[§], E. Chen[♦], B. Verlinden[♦] and A.M. Habraken[‡]
[‡] ARGENCO Department, University of Liège, Belgium
§ Dept. of Mechanical Engineering, Eindhoven University of Technology, The Netherlands
♦ Dept. of Materials Engineering, Katholieke Universiteit Leuven, Belgium

ABSTRACT

The Equal Channel Angular Extrusion process is used to modify the microstructure of an AA1050 aluminum alloy in order to produce an ultra fine grained material. Due to the severe plastic deformation undergone by the material during the ECAE process, the subsequent behavior of the material is non-conventional and difficult to model with classical constitutive laws (e.g. ECAE aluminum presents a large initial back-stress which must be adequately incorporated in the model). In this study, the evolution of the back-stress during the ECAE process is analyzed. Two different numerical models were investigated in this respect. The first one is a single crystal strain gradient plasticity model based on dislocation densities. The second model is the Teodosiu and Hu's hardening model, which is a microstructuraly based phenomenological model at the macroscale. The results provided by the two models are obviously distinct. Nevertheless, some common trends can be pointed out, among which the amplitude of the back-stress that is similar. In agreement with the cyclic deformation mode of the studied route C ECAE process, the evolution of the predicted back-stress is also cyclic in both models.

INTRODUCTION

The Equal Channel Angular Extrusion (ECAE) process is used in the present study to produce ultra fine grained aluminum. It is well-known that a decrease in the grain size of a material is accompanied by an increase of the yield strength as can be represented by the Hall-Petch relation [1]. Due to their particular mechanical properties, an increasing interest is currently dedicated to the study of ultra fine grained materials. However, the modeling of these materials is not straightforward. The material deformed by the ECAE process is far from its virgin state. Very large plastic strains (in the studied case, the plastic equivalent strain is 1.15 per pass) are imposed to the material.

In the framework of this study, several mechanical tests were performed on the aluminum produced by ECAE in order to assess its mechanical behavior [2]. It appeared that a significant kinematic hardening was observed. Furthermore, the ECAE aluminum presented an initial back-stress resulting from the deformation that occurred during the ECAE process.

This contribution assesses the performance of two different numerical models for an accurate modeling of ECAE processed aluminum. A single crystal strain gradient plasticity model was scrutinized in this respect. This model uses as internal variables the densities of statistically stored dislocations (SSD) and geometrically necessary dislocations (GND). The evolution of the SSD densities is based on a balance between dislocation accumulation and annihilation rates depending on the slip rates. The GND densities on the other hand result from the incompatibilities in the crystal lattice due to gradient of the dislocation slip. Both GND and

SSD densities are taken into account for the isotropic hardening of the material. The GND densities naturally induce a physically based kinematic hardening through their internal stresses (i.e. the back-stress, computed as a function of the GND densities gradient).

In addition, a macroscopic phenomenological hardening model was investigated. The Teodosiu and Hu's hardening model [3;4] is a physically-based microstructural model. Basically, it is able to describe both kinematic and isotropic hardening, reflecting the influence of the dislocation structures and their evolutions, at a macroscopic scale. It permits to describe complex hardening behaviors induced by strain-path changes.

The goals of this research are multiple. First, different numerical models were used to predict the evolution of the back-stress during an ECAE process. This yields new insights and more accurate material parameters as used in phenomenological models adapted to ECAE materials (mainly a reasonable initial back-stress). The modeling of the ECAE process also results in an improved knowledge of the mechanisms involved during this forming process. Finally, this research permits the comparison of two promising yet different models with very different approaches on a relevant application.

THE MODELS

Strain gradient crystal plasticity model

The constitutive framework of this model departs from the classical multiplicative decomposition of the deformation gradient $\mathbf{F}$ into a plastic part $\mathbf{F}_p$ and an elastic part $\mathbf{F}_e$:

$$\mathbf{F} = \mathbf{F}_e \cdot \mathbf{F}_p \tag{1}$$

$\mathbf{F}_p$ is assumed to be achieved only by dislocation slip. $\mathbf{F}_e$ includes small lattice deformation and (possibly) large rigid body rotations. The elastic behavior of the material is determined by equation (2), where $\mathbf{S}$ is the second Piola-Kirchhoff stress tensor expressed in the stress-free intermediate configuration (the material deformed by $\mathbf{F}_p$ only), ${}^4\mathbf{C}$ is the fourth order anisotropic elasticity tensor (it is defined by three material parameters, which are three of its components: C_{11},C_{12},C_{44}). $\mathbf{E}_e$ is the Green-Lagrange elastic strain (work-conjugated to $\mathbf{S}$), obtained by $\mathbf{E}_e = \frac{1}{2}\left(\mathbf{F}_e^{\mathrm{T}} \cdot \mathbf{F}_e - \mathbf{I}\right)$.

$$\mathbf{S} = {}^4\mathbf{C} : \mathbf{E}_e \tag{2}$$

The plastic deformation is due to dislocation glide on slip systems. Therefore, the plastic velocity gradient tensor (related to the plastic part of the deformation gradient by $\dot{\mathbf{F}}_p = \mathbf{L}_p \cdot \mathbf{F}_p$) is expressed in the form:

$$\mathbf{L}_p = \sum_{\alpha=1}^{12} \dot{\gamma}^{\alpha} \mathbf{P}_0^{\alpha} \tag{3}$$

In equation (3), $\dot{\gamma}^{\alpha}$ is the slip rate on slip system α, the non-symmetric Schmid tensors are defined by $\left(\mathbf{P}_0^{\alpha}\right)_{ij} = \left(\vec{s}_0^{\alpha}\right)_i \left(\vec{n}_0^{\alpha}\right)_j$, with $\vec{s}_0^{\alpha}$ and $\vec{n}_0^{\alpha}$ the slip direction and the slip plane normal for the slip system α (expressed in the undeformed configuration).

A visco-plastic slip law relates the slip rates to the effective stresses τ_{eff}^{α}:

$$\dot{\gamma}^{\alpha} = \dot{\gamma}_0 \left| \frac{\tau^{\alpha}_{eff}}{s^{\alpha}} \right|^{1/m} \exp\left(-\frac{G_0}{kT}\left(1 - \left| \frac{\tau^{\alpha}_{eff}}{s^{\alpha}} \right| \right) \right) sign\left(\tau^{\alpha}_{eff} \right) \tag{4}$$

$\dot{\gamma}_0$, m, G_0 are material parameters; k is the Boltzmann's constant and T is the absolute temperature. In equation (4), the exponential term represents the thermally induced dislocation motion. The effective stresses τ^{α}_{eff} are obtained from equation (5), where τ^{α} are the Schmid stresses defined as the resolved part of the second P-K stress on the slip systems $\tau^{\alpha} = \mathbf{S} : \mathbf{P}^{\alpha}_0$.

$$\tau^{\alpha}_{eff} = \tau^{\alpha} - \tau^{\alpha}_{b} \tag{5}$$

τ^{α}_{b} is the back-stress related to the kinematic hardening included in this model. It is the resolved part of the internal stresses induced by the edge and screw dislocation densities present on all slip systems according to equation (6).

$$\tau^{\alpha}_{b} = -\left(\boldsymbol{\sigma}^{int}_{e} + \boldsymbol{\sigma}^{int}_{s} \right) : \mathbf{P}^{\alpha}_0 \tag{6}$$

The presence of dislocations in the crystal creates a deformation of the lattice. Assuming (at this stage only) that the material is an isotropic elastic continuum medium, the internal stresses resulting from distributions of dislocation densities take the form of equation (7) for edge dislocations and equation (8) for screw dislocations.

$$\boldsymbol{\sigma}^{int}_{e} = \frac{GbR_e^2}{8(1-\nu)} \sum_{\xi=1}^{12} \vec{\nabla}_0 \rho^{\xi}_{GND} \cdot \left(3\vec{n}^{\xi}_0 \vec{s}^{\xi}_0 \vec{s}^{\xi}_0 - \vec{s}^{\xi}_0 \vec{s}^{\xi}_0 \vec{n}^{\xi}_0 - \vec{s}^{\xi}_0 \vec{n}^{\xi}_0 \vec{s}^{\xi}_0 + \vec{n}^{\xi}_0 \vec{n}^{\xi}_0 \vec{n}^{\xi}_0 + 4\nu \vec{n}^{\xi}_0 \vec{p}^{\xi}_0 \vec{p}^{\xi}_0 \right) \tag{7}$$

$$\boldsymbol{\sigma}^{int}_{s} = \frac{GbR_s^2}{4} \sum_{\xi=13}^{18} \vec{\nabla}_0 \rho^{\xi}_{GND} \cdot \left(-\vec{n}^{\xi}_0 \vec{s}^{\xi}_0 \vec{p}^{\xi}_0 - \vec{n}^{\xi}_0 \vec{p}^{\xi}_0 \vec{s}^{\xi}_0 + \vec{p}^{\xi}_0 \vec{s}^{\xi}_0 \vec{n}^{\xi}_0 + \vec{p}^{\xi}_0 \vec{n}^{\xi}_0 \vec{s}^{\xi}_0 \right), \quad with \quad \vec{p}^{\xi}_0 = \vec{s}^{\xi}_0 \times \vec{n}^{\xi}_0 \tag{8}$$

In equations (7) and (8), G is the (isotropic) shear modulus, ν is Poisson's ratio, b is the length of the Burgers vector and R_e and R_s are the radii of the fictitious spherical domain (around the point where the internal stresses are computed) limiting the dislocations taken into consideration. It should be noted at this stage that the dislocation densities are separated in two categories: the geometrically necessary dislocations (GND) and the statistically stored dislocations (SSD). The GNDs are generated during the plastic deformation by dislocation glide in order to maintain the compatibility of the crystal lattice. They have a specific orientation (depending on the slip on each slip system) and, they therefore have a net contribution to the internal stresses. On the other hand, the SSD have a random orientation such that their influence on the internal stresses vanishes. It appears in equations (7) and (8) that the gradient of the GND densities ρ^{ξ}_{GND} is the governing quantity for the internal stresses. The present crystal plasticity model considers face centered cubic metals having 12 slip systems and, consequently, 12 edge dislocations and 6 screw dislocations families are considered. In equation (4), the slip resistance s^{α} is still not defined. It is related to the local slip system hardening. The slip resistance evolves as a function of GND and SSD densities through equation (9).

$$s^{\alpha} = cGb \sqrt{ \sum_{\xi=1}^{12} A^{\alpha\xi} \left| \rho^{\xi}_{SSD} \right| + \sum_{\xi=1}^{18} A^{\alpha\xi} \left| \rho^{\xi}_{GND} \right| } \tag{9}$$

c is a material constant and $A^{\alpha\xi}$ are interaction parameters between slip system α and dislocation ξ. The evolution rule for the SSD densities results from a competition between an accumulation rate and an annihilation rate:

$$\dot{\rho}_{SSD}^{\xi} = \frac{1}{b}\left(\frac{1}{L^{\xi}} - 2y_c\rho_{SSD}^{\xi}\right)\left|\dot{\gamma}^{\xi}\right| \tag{10}$$

with
$$L^{\alpha} = \frac{K}{\sqrt{\sum_{\xi=1}^{12} H^{\alpha\xi}\left|\rho_{SSD}^{\xi}\right| + \sum_{\xi=1}^{18} H^{\alpha\xi}\left|\rho_{GND}^{\xi}\right|}} \tag{11}$$

and an initial condition:
$$\rho_{SSD}^{\xi}\left(t=0\right) = \left(\rho_{SSD}^{\xi}\right)_0 \tag{12}$$

In equations (10) to (12), y_c, K and $\left(\rho_{SSD}^{\xi}\right)_0$ are material parameters; $H^{\alpha\xi}$ is an interaction matrix (similar to $A^{\alpha\xi}$) and t is the time.

The GND densities evolution is based on the geometrical compatibility of the crystal lattice during plastic deformation. The GND are introduced to maintain the lattice continuity in the crystals in spite of the dislocation slips. The evolution rules are:

$$\rho_{GND}^{\xi} = \left(\rho_{GND}^{\xi}\right)_0 - \frac{1}{b}\vec{\nabla}_0\gamma^{\xi}\cdot\vec{s}_0^{\xi} \tag{13}$$

$$\rho_{GND}^{\xi} = \left(\rho_{GND}^{\xi}\right)_0 + \frac{1}{b}\left(\vec{\nabla}_0\gamma^{\alpha_1}\cdot\vec{p}_0^{\alpha_1} + \vec{\nabla}_0\gamma^{\alpha_2}\cdot\vec{p}_0^{\alpha_2}\right) \tag{14}$$

for edge GND densities (ξ=1…12) and screw GND densities (ξ=13…18), respectively.

Further details about the strain gradient crystal plasticity model can be found in [5-8].

Teodosiu and Hu's hardening model

Teodosiu and Hu's hardening model is described by 13 material parameters:

$$C_p, C_R, C_{Sd}, C_{SL}, C_X, f, n_L, n_P, r, Y_0, R_{Sat}, S_{sat}, X_0 \tag{15}$$

and depends on four state variables:

$$\mathbf{P}, \mathbf{S}, \mathbf{X}, R \tag{16}$$

Variable **P** is a second-order tensor that depicts the polarity of the persistent dislocation structures (PDSs in [9]) and **S** is a fourth-order tensor that describes the directional strength of the PDSs. Scalar R represents the isotropic hardening due to randomly distributed dislocations and the second-order tensor **X** is the back-stress. These state variables evolve with respect to the plastic strain rate $\dot{\boldsymbol{\varepsilon}}^p$ and the equivalent plastic strain rate $\dot{p}$ as given by

$$\dot{Y} = f_Y\left(Y, \dot{\boldsymbol{\varepsilon}}^p\right)\dot{p} \tag{17}$$

A precise description of these evolution equations can be found in [3;10-11]. It should however be noticed that the fourth-order tensor **S** must be decomposed into S_D and $\mathbf{S}_L$ according to Equation (18). S_D is the strength of the dislocation structure associated with the currently

active slip systems and $\mathbf{S}_L$ is the latent part of $\mathbf{S}$ related to the persistent dislocation structure associated with the latent slip systems.

$$\mathbf{S} = S_D \mathbf{N}_{\dot{\varepsilon}^p} \otimes \mathbf{N}_{\dot{\varepsilon}^p} + \mathbf{S}_L \tag{18}$$

where $\mathbf{N}_{\dot{\varepsilon}^p}$ is the plastic strain rate direction. Two distinct evolution equations (with the form of Equation (17)) are applied to S_D and $\mathbf{S}_L$.

The yield condition is given by Equation (19).

$$\bar{\sigma} = \sigma_y = Y_0 + R + f\,|\mathbf{S}| \tag{19}$$

where $\bar{\sigma}$ is the equivalent stress, function of $\mathrm{dev}(\boldsymbol{\sigma}) - \mathbf{X}$, σ_y is the current elastic limit, Y_0 is the initial size of the yield locus and $R + f\,|\mathbf{S}|$ represents the evolution of the isotropic hardening. The expression of $\bar{\sigma}$ depends on the definition of the yield locus.

MODELING THE ECAE PROCESS

The ECAE process is schematically represented in Figure 1. In this study, the material (one material point is illustrated by the square in Figure 1) was assumed to be submitted to simple shear in the intersection plane of the two channels. In this respect, the numerical simulations were defined in a reference system attached to that plane. The material was submitted to the ECAE process following route C (180° rotation of the sample between each pass) for 4 passes. This route can be modeled by simple shear (with a shear strain ranging from 0 to 2 for the studied ECAE geometry) for the first pass and reversed shear for the second pass. The initial shape of the material is recovered every 2 passes.

For the strain gradient crystal plasticity law, the orientations of the individual grains are required as input data. The texture of the aluminum before the ECAE process was used to extract a set of 8 representative orientations. The grains with these orientations were submitted to simple shear separately (Taylor analysis). The material parameters for the strain gradient crystal plasticity model were largely extracted from [6] and [12]. Only the initial SSD densities $\left(\rho^{\xi}_{SSD}\right)_0$ were adjusted according to the actual hardening behavior of the studied aluminum. A value of 400 μm^{-2} was adopted.

For the Teodosiu and Hu's model, the material parameters for the aluminum were obtained from [13].

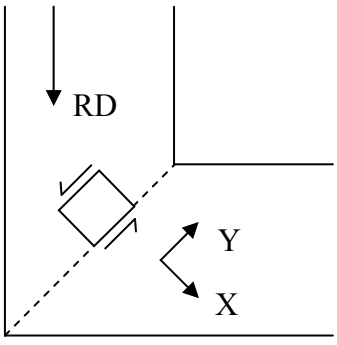

Figure 1. Schematic representation of the ECAE process (RD is the rolling direction of the initial material).

NUMERICAL RESULTS

Figure 2 presents the evolution of the shear stress as a function of the shear strain with the strain gradient crystal plasticity model during the ECAE process following route C for 4 passes. The Bauschinger effect can be observed at the load reversal between successive passes. The kinematic hardening (linked to the back-stress) is at the origin of this effect in the model.

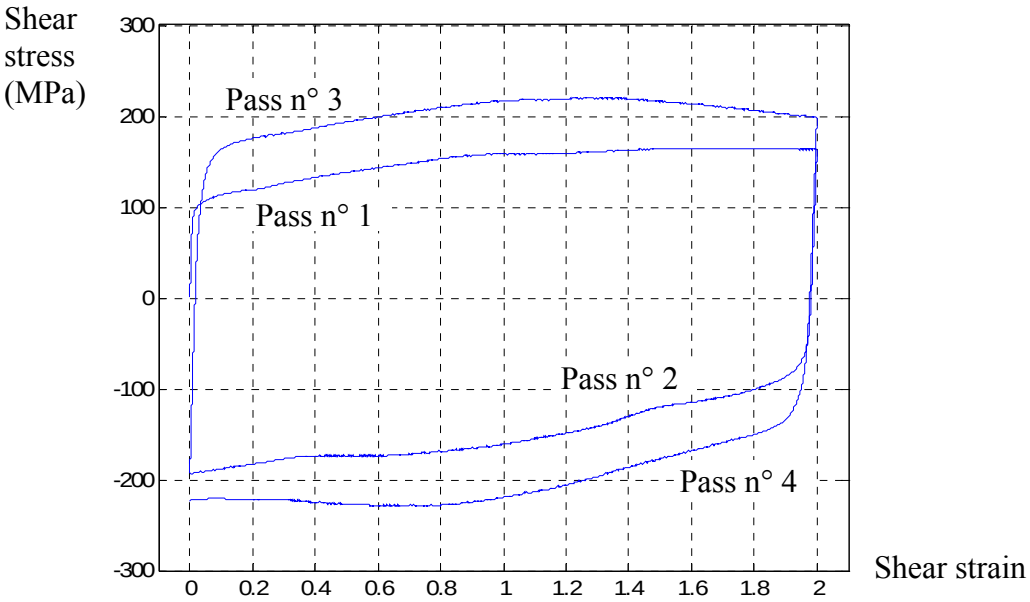

Figure 2. Shear stress – shear strain during ECAE process for 4 passes (route C).

The evolution of the back-stress during the 4 passes is plotted in Figure 3. The back-stress at the centre of each grain is next considered in more detail. The mean value over the 8 grains of the representative set is shown. The maximum values for the back-stress were obtained after the first and the third passes. Lower values were noticed after 2 and 4 passes. This result is confirmed by the amplitude of the Bauschinger effect between the successive passes in Figure 2. Due to the repetitive aspect of the route C, it was expected (and confirmed) that the material behavior during the first and the second passes was similar to the one during the third and fourth passes. By comparing Figures 2 and 3, it appears that the amplitude of the back-stress is a fraction (around a fifth) of the shear stress.

Figure 4 presents the evolution of the back-stress calculated with the Teodosiu and Hu's hardening model. The overall amplitude of the back-stress as predicted by Teodosiu and Hu's model is similar to the amplitude with the crystal plasticity model. On the other hand, a very different evolution of each component was observed, i.e. the orientation of the back-stress is very different. Again, a repetition (more strict in this case) of the two first passes appeared during the two last passes. Besides, an abrupt evolution of the back-stress was observed during the first stage of the reversed shearing (beginning of passes 2 and 4). At the end of passes 2 and 4, only the shear component ($_{12}$) of the back-stress remains.

CONCLUSIONS

During this study, two different models (microscopic and macroscopic) were investigated for the numerical prediction of the back-stress (kinematic hardening) during the ECAE process following route C for 4 passes. The two models yield different results in terms of the evolution of the back-stress while a similar amplitude was observed.

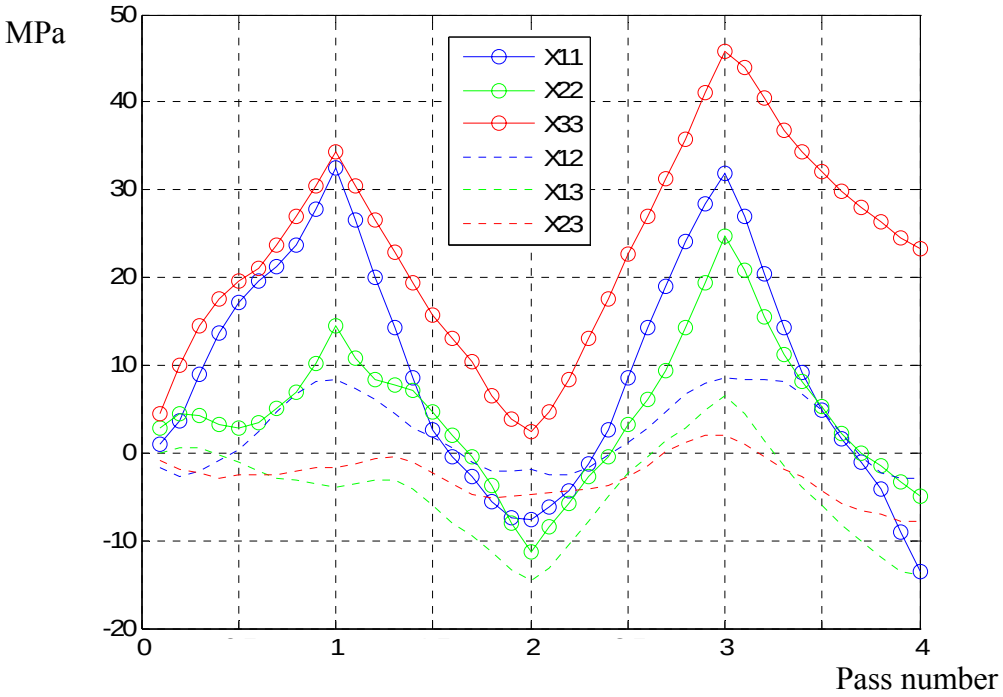

Figure 3. Evolution of the back-stress (**X**) during the ECAE process for 4 passes (route C) with the strain gradient crystal plasticity model. The components of **X** are expressed in the reference frame of Fig. 1.

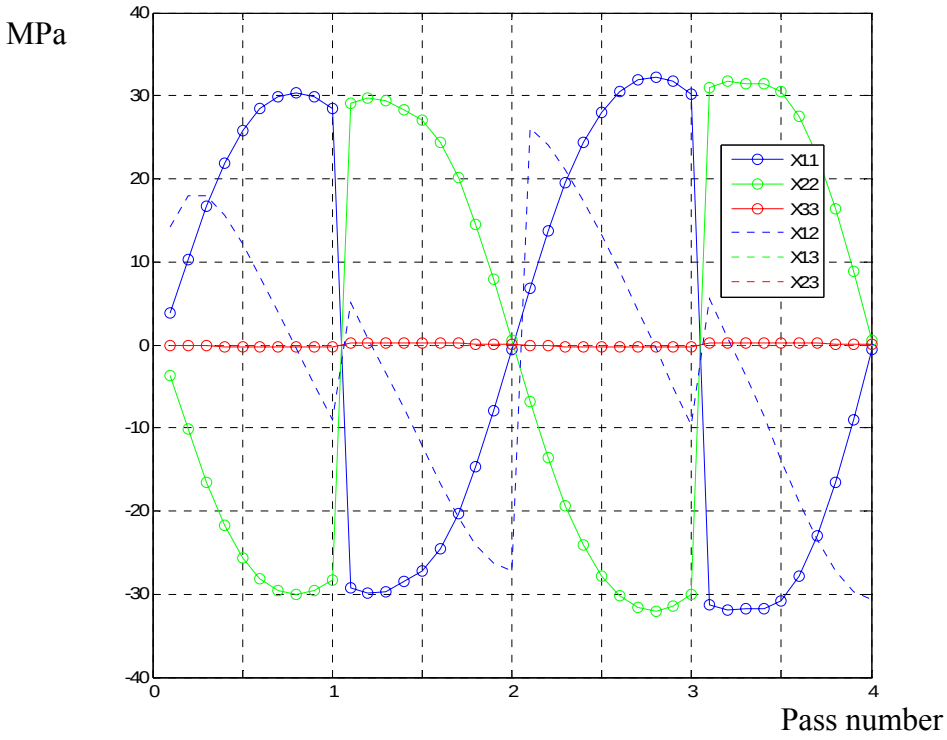

Figure 4. Evolution of the backstress (**X**) during the ECAE process for 4 passes (route C) with the Teodosiu and Hu's hardening model. The components of **X** are expressed in the reference frame of Fig. 1.

The difference between the two models can be partly explained by the microscopic and macroscopic aspects of these models. On the one hand, for the strain gradient crystal plasticity model, the back-stress originates from a gradient of the GND densities inside each grain. This gradient is mainly due to the presence of the grain boundaries. On the other hand, a homogeneous behavior is assumed with the Teodosiu and Hu's model. More consistently, both models predicted a larger overall back-stress after passes 1 and 3 and a lower value after 2 and 4 passes. This observation should be checked experimentally.

ACKNOWLEDGEMENTS

The authors acknowledge the Interuniversity Attraction Poles Programme - Belgian State – Belgian Science Policy (Contract P6/24). A.M.H. and L.D. also acknowledge the Belgian Fund for Scientific Research FRS-FNRS for its support.

REFERENCES

1. Hall, E.O., The deformation and aging of mild steel: iii. Discussion of results. *Proc. Physical Society of London*, **B64**, 747-753 (1951).
2. Poortmans, S. and Verlinden, B., Mechanical properties of fine-grained AA1050 after ECAP. *Materials Science Forum* **503-504**, 847-852 (2006).
3. Teodosiu, C., Hu, Z., Evolution of the intragranular microstructure at moderate and large strains: modeling and computational significance. *In Proc. NUMIFORM 95,* edited by Shen, S.F. and Dawson, P.R., pp. 173-182 (1995).
4. Bouvier, S., Teodosiu, C., Haddadi, H. and Tabacaru, V., Anisotropic Work-Hardening Behaviour of Structural Steels and Aluminium Alloys at Large Strains. *In: Proc. of the Sixth European Mechanics of Material Conference (EMMC6)*, S. Cescotto Eds, 329-336 (2002).
5. Evers, L.P., Brekelmans, W.A.M., Geers, M.G.D., Non-local crystal plasticity model with intrinsic SSD and GND effects. *J. of the Mechanics and Physics of Solids*, **52**, 2379-2401 (2004).
6. Evers, L.P., Brekelmans, W.A.M., Geers, M.G.D., Scale dependent crystal plasticity framework with dislocation density and grain boundary effects. *International Journal of solids and structures*, **41**, 5209-5230 (2004).
7. Bayley, C.J., Brekelmans, W.A.M., Geers, M.G.D., A comparison of dislocation induced back stress formulations in strain gradient crystal plasticity. *International Journal of Solids and Structures*, **43**, 7268-7286 (2006).
8. Bayley, C.J., Brekelmans, W.A.M., Geers, M.G.D., A three-dimensional field crystal plasticity approach applied to miniaturized structures. *Philosophical Mag.*, **87** (8-9), 1361-1378 (2007).
9. Li, S., Hoferlin, E., Van Bael, A., Van Houtte, P., Teodosiu, C., *Int. J. Plast.* **19**, 647-674 (2003).
10. Bouvier, S., Alves, J.L., Oliveira, M.C., Menezes, L.F., *Comp. Mater. Sci.* **32**, 301-315 (2005).
11. Alves, J.L., Oliveira, M.C., Menezes, L.F., An advanced constitutive model in sheet metal forming simulation: the Teodosiu microstructural model and the Cazacu Barlat yield criterion. *In Proc. NUMIFORM*, edited by Ghosh, S. et al., AIP Conf. Proc. 712, pp. 1645-1650 (2004).
12. Fülöp, T., Brekelmans, W.A.M., Geers, M.G.D., Size effects from grain statistics in ultra-thin metal sheets. *Journal of Materials Processing Technology* **174**, 233-238 (2006).
13. Flores, P., Duchêne, L., Bouffioux, C., Lelotte, T., Henrard, C., Pernin, N., Van Bael, A., He, S., Duflou, J., Habraken, A.M., Model Identification and FE Simulations: Effect of Different Yield Loci and Hardening Laws in Sheet Forming. *Int. J. of Plasticity*, **23** (3), 420-449 (2007).